Generalized quantum geometric tensor and its properties in disordered lattices

Yihan Chen(陈亦涵), Tao Qin(秦涛)

Citation: Chin. Phys. B. 35, 100302 (2026). DOI: 10.1088/1674-1056/ae838d | CSTR: 32038.14.CPB.ae838d
http://cpb.iphy.ac.cn; http://iopscience.iop.org/cpb

What follows is a list of articles you may be interested in

Interplay between topology and localization on superconducting circuits

Xin Guan(关欣), Bingyan Huo(霍炳燕), Gang Chen(陈刚)
Chin. Phys. B. 33, 060311 (2024). DOI: 10.1088/1674-1056/ad342c

Observation of flat-band localized state in a one-dimensional diamond momentum lattice of ultracold atoms

Chao Zeng(曾超), Yue-Ran Shi(石悦然), Yi-Yi Mao(毛一屹), Fei-Fei Wu(武菲菲), Yan-Jun Xie(谢岩骏), Tao Yuan(苑涛), Han-Ning Dai(戴汉宁), Yu-Ao Chen(陈宇翱)
Chin. Phys. B. 33, 010303 (2024). DOI: 10.1088/1674-1056/ad0cd1

Periodic electron oscillation in coupled two-dimensional lattices

Yan-Yan Lu(陆艳艳), Chao Wang(王超), Jin-Yi Jiang(将金益), Jie Liu(刘洁), Jian-Xin Zhong(钟建新)
Chin. Phys. B. 32, 070306 (2023). DOI: 10.1088/1674-1056/acce93

Engineering topological state transfer in four-period Su–Schrieffer–Heeger chain

Xi-Xi Bao(包茜茜), Gang-Feng Guo(郭刚峰), Lei Tan(谭磊)
Chin. Phys. B. 32, 020301 (2023). DOI: 10.1088/1674-1056/ac7bfe

Filling up complex spectral regions through non-Hermitian disordered chains

Hui Jiang, Ching Hua Lee
Chin. Phys. B. 31, 050307 (2022). DOI: 10.1088/1674-1056/ac4a73

RAPID COMMUNICATION

Generalized quantum geometric tensor and its properties in disordered lattices

Yihan Chen(陈亦涵) and Tao Qin(秦涛)†

School of Physics, Anhui University, Hefei 230601, *China*

(Received 8 May 2026; revised manuscript received 20 June 2026; accepted manuscript online 29 June 2026)

Recent investigations into the role of the quantum geometric tensor (QGT) in exotic condensed matter phenomena have attracted considerable attention. However, the conventional QGT only captures the geometry of the Bloch states, leaving out contributions from non-trivial physical quantities such as magnetizations. We therefore generalize the conventional QGT to incorporate the orbital magnetization, energy magnetization, and Drude weight. To address the influence of disorder on these tensors, we further develop a set of real-space formulas for the generalized QGTs. Using the Haldane model as an example, we demonstrate that the semi-positive definiteness of these tensors still enforces meaningful constraints. Moreover, the real-space formulation provides a basis for studying more intriguing cases involving various types of disorder.

Keywords: generalized quantum geometric tensors, disorders, semi-positive definite

PACS: 03.65.Vf, 42.25.Ja, 71.27.+a

DOI: 10.1088/1674-1056/ae838d **CSTR:** 32038.14.CPB.ae838d

1. Introduction

The quantum geometric tensor, with its real and imaginary parts as the quantum metric[1,2] and Berry curvature[3] encoding the amplitude distance and phase distance between quantum states,[4] respectively, plays a central role in emergent transport phenomena in condensed matter physics.[5–7] On one hand, exploring exotic effects of the quantum metric has garnered considerable attention recently,[8] with the focus on the nonlinear Hall effect,[9,10] the connection with bulk electron–phonon coupling,[11] superfluid density in flat-band superconductivity[12] and so on. On the other hand, the semi-positive definite properties impose non-trivial constraints on the quantum geometric tensor (QGT), indicating meaningful physical bounds.[13–16] Furthermore, disorder effects on QGT in the two-band model have been studied with the perturbation method[17] and the numerical method.[18] We point out that work on quantum geometry in two respects is still lacking. Firstly, a further generalization to include orbital magnetization[19] and energy magnetization[20] is necessary to investigate the anomalous (thermal) Hall effect from the point of view of generalized quantum geometry. Secondly, a systematic study of disorder effects on QGT and its generalizations remains absent, leaving a critical gap in understanding the physics induced by ubiquitous impurities.

Here, we further generalize the definition of the QGT. With the generalization of the definition of the QGT to include the orbital magnetization,[19] energy magnetization,[20] and Drude weight,[21] intriguing transport phenomena can be discussed in a uniform frame. With the semi-positive definiteness properties of the generalized quantum geometric tensors (GQGT), we put forward the inequalities satisfied by the real and imaginary parts, which are supposed to be valid in a clean bulk system. However, whether these inequalities still work in disordered lattices is an interesting and open question. To this end, we develop a group of real-space formulas, focusing on both the imaginary[22] and real parts, and perform a systematic calculation of the GQGTs in disordered lattices. With the Haldane model[23] as an example, we demonstrate that these inequalities are still effective constraints.

The remainder of the manuscript is organized as follows. In Section 2, we present the definitions for the GQGT in momentum space, and its properties due to the semi-positive definiteness. In Section 3, we give the real-space formalism for GQGTs, which makes it possible to carry out the calculations in disordered lattices. In Section 4, we present the model and methods, and in Section 5, we provide results of GQGT of the Haldane model in disordered lattices. Finally, in Section 6, we make a brief summary and outlook.

2. Generalized quantum geometric tensors

We put forward a set of GQGTs for non-interacting electrons as a generalization of the QGT in a lattice

$$\mathcal{Q}^{(j)}_{\alpha\beta} = \mathcal{R}^{(j)}_{\alpha\beta} + \mathrm{i}\mathcal{I}^{(j)}_{\alpha\beta}, \tag{1}$$

†Corresponding author. E-mail: taoqin@ahu.edu.cn

© 2026 Chinese Physical Society and IOP Publishing Ltd. All rights, including for text and data mining, AI training, and similar technologies, are reserved.

where we have defined the real part as

$$\mathcal{R}^{(j)}_{\alpha\beta} = \frac{1}{\pi}\mathrm{Re}\sum_{n\in\mathrm{occ},\boldsymbol{k}}\left\langle \partial_{k_\beta}u_{n\boldsymbol{k}}\right| Q_{\boldsymbol{k}}\left(\tilde{H}_{\boldsymbol{k}}-\tilde{\varepsilon}_{n\boldsymbol{k}}\right)^{j} Q_{\boldsymbol{k}}\left|\partial_{k_\alpha}u_{n\boldsymbol{k}}\right\rangle, \quad (2)$$

and the imaginary part as

$$\mathcal{I}^{(j)}_{\alpha\beta} = \frac{1}{\pi}\mathrm{Im}\sum_{n\in\mathrm{occ},\boldsymbol{k}}\left\langle \partial_{k_\beta}u_{n\boldsymbol{k}}\right| Q_{\boldsymbol{k}}\left(\tilde{H}_{\boldsymbol{k}}+\tilde{\varepsilon}_{n\boldsymbol{k}}\right)^{j} Q_{\boldsymbol{k}}\left|\partial_{k_\alpha}u_{n\boldsymbol{k}}\right\rangle. \quad (3)$$

Here, "occ" denotes occupied states, the projector operator $Q_{\boldsymbol{k}}=\sum_{n\notin\mathrm{occ}}|u_{n\boldsymbol{k}}\rangle\langle u_{n\boldsymbol{k}}|$, and $|u_{n\boldsymbol{k}}\rangle$ is the periodic part of the Bloch states for energy band n with momentum $\boldsymbol{k}$. $\tilde{H}_{\boldsymbol{k}}=H_{\boldsymbol{k}}-\mu$ with $H_{\boldsymbol{k}}$ being the electron Hamiltonian, μ being the chemical potential, and $\tilde{\varepsilon}_{n\boldsymbol{k}}=\varepsilon_{n\boldsymbol{k}}-\mu$ with $\varepsilon_{n\boldsymbol{k}}$ being the eigen-energy. We focus on a two-dimensional lattice with $\alpha,\beta\in\{x,y\}$ and $\partial_{k_\alpha}=\partial/\partial k_\alpha$. We set $j=0,1,2$, corresponding to different physical quantities. $\mathcal{I}^{(j)}_{xx}=\mathcal{I}^{(j)}_{yy}=0$. Both the real and imaginary parts have a clear hierarchy structure.

We discuss the physical meaning of $\mathcal{Q}^{(j)}_{\alpha\beta}$ for $j=0,1,2$. Clearly, $\mathcal{Q}^{(0)}_{\alpha\beta}$ is the usual quantum geometric tensor,[8] with the real and imaginary parts as the quantum metric and Berry curvature, respectively. The off-diagonal imaginary part $\mathcal{I}^{(1)}_{\alpha\beta}$ is effectively the orbital magnetization at zero temperature[19], and the real part $\mathcal{R}^{(1)}_{\alpha\beta}$ is the inter-band Drude weight.[24] We further point out that the off-diagonal imaginary part of $\mathcal{I}^{(2)}_{\alpha\beta}$ is, in fact, the energy magnetization at zero temperature.[20] Meanwhile, we term the real part $\mathcal{R}^{(2)}_{\alpha\beta}$ as the inter-band energy Drude weight. While $j=0,1$ has been studied in Ref. [24], the case of $j=2$ is systematically studied in this work.

We comment on semi-positive definite properties of $\mathcal{Q}^{(j)}_{\alpha\beta}$. For $j=0,1$, it has been proved in Ref. [24] that $\mathcal{Q}^{(j)}_{\alpha\beta}=\frac{1}{\pi}\sum_{\boldsymbol{k}}\mathrm{Tr}\left[O^{(j)}_{\boldsymbol{k}}\left(\partial_{k_\alpha}P_{\boldsymbol{k}}\partial_{k_\beta}P_{\boldsymbol{k}}\right)\right]$, with $P_{\boldsymbol{k}}=\sum_{n\in\mathrm{occ}}|u_{n\boldsymbol{k}}\rangle\langle u_{n\boldsymbol{k}}|$, where $O^{(1)}_{\boldsymbol{k}}=P_{\boldsymbol{k}}$, and $O^{(2)}_{\boldsymbol{k}}=\tilde{H}_{\boldsymbol{k}}(I-2P_{\boldsymbol{k}})$ with I being the identity operator. $\mathcal{Q}^{(j)}_{\alpha\beta}$ for $j=0,1$ is semi-positive definite, which states that

$$\sqrt{\det\left[\mathcal{R}^{(j)}_{\alpha\beta}\right]}\geq\left|\mathcal{I}^{(j)}_{xy}\right|. \quad (4)$$

Even though both the real and imaginary parts have a clear hierarchy structure, in general $\mathcal{Q}^{(2)}_{\alpha\beta}$ is not semi-positive definite. With the Cauchy–Schwarz inequality, one can show the real part is semi-positive definite, but the imaginary part is not.

3. Real space formalism

What is the fate of Eq. (4) for $j=0,1$ if onsite disorders are introduced? What are the effects of onsite disorders on these physical quantities? To this end, we introduce a real-space formalism for $\mathcal{Q}^{(j)}_{\alpha\beta}$ in Eq. (1). We first present the real-space formulas as follows:

$$\mathcal{Q}^{(0)}_{\alpha\beta} = -\frac{4\pi}{A_{\mathrm{c}}}\mathrm{Tr}\left(\hat{P}r_\alpha\hat{Q}r_\beta\hat{P}\right), \quad (5)$$

$$\mathcal{Q}^{(1)}_{\alpha\beta} = -\frac{4\pi}{A_{\mathrm{c}}}\mathrm{Tr}\left(Pr_\alpha Q\tilde{H}Qr_\beta P-Qr_\alpha P\tilde{H}Pr_\beta Q\right), \quad (6)$$

$$\mathcal{Q}^{(2)}_{\alpha\beta} = -\frac{4\pi}{A_{\mathrm{c}}}\mathrm{Tr}\big(Pr_\alpha\tilde{H}^2Qr_\beta P+Pr_\alpha Qr_\beta\tilde{H}^2P -2P\tilde{H}r_\beta Q\tilde{H}r_\alpha P\big). \quad (7)$$

Here $\alpha,\beta\in\{x,y\}$, and $\tilde{H}=H-\mu$ with H being the real-space Hamiltonian. A_{c} is the area of a unit cell in the two-dimensional case we have considered. The trace Tr is over all the lattice sites. $P=\sum_{\varepsilon_n<\mu}|n\rangle\langle n|$ and $Q=I-P$. $r_\alpha=\mathrm{diag}\,[r_{1\alpha},\ldots,r_{N\alpha}]$ with N being the number of all the lattice sites considered. Surprisingly, in real space, there are unified formulas for all the cases of j. Similar formulas have been developed in Ref. [22], which specifically focused on the imaginary part.

Since the real-space formalisms for the imaginary parts of $\mathcal{Q}^{(j)}_{\alpha\beta}$ with $j=0,1$ have been developed in Refs. [25,26], we focus on the derivation details for the case of $j=2$. We start with $\mathcal{I}^{(2)}_{xy}$, which is the energy magnetization introduced in Ref. [20] as

$$\mathcal{I}^{(2)}_{xy}=-\frac{1}{\pi}\mathrm{Im}\int_{\mathrm{BZ}}\mathrm{d}\boldsymbol{k}\sum_{n\in\mathrm{occ}}\left\langle\frac{\partial u_{n\boldsymbol{k}}}{\partial k_x}\right|\left(\tilde{H}+\tilde{\varepsilon}_{n\boldsymbol{k}}\right)^2\left|\frac{\partial u_{n\boldsymbol{k}}}{\partial k_y}\right\rangle.$$

By inserting the projector operator $Q_{\boldsymbol{k}}$, we have

$$\mathcal{I}^{(2)}_{xy} = -\frac{1}{\pi}\mathrm{Im}\int_{\mathrm{BZ}}\mathrm{d}\boldsymbol{k}\sum_{n\in\mathrm{occ}}\sum_{n'\notin\mathrm{occ}}\left(\tilde{\varepsilon}_{n'\boldsymbol{k}}+\tilde{\varepsilon}_{n\boldsymbol{k}}\right)^2\left\langle\frac{\partial u_{n\boldsymbol{k}}}{\partial k_x}\right|u_{n'\boldsymbol{k}}\right\rangle\left\langle u_{n'\boldsymbol{k}}\right|\left.\frac{\partial u_{n\boldsymbol{k}}}{\partial k_y}\right\rangle. \quad (8)$$

With the identity,[27] $\langle\psi_{n'\boldsymbol{k}}|r_\alpha|\psi_{n\boldsymbol{k}}\rangle=\frac{(2\pi)^2}{A_{\mathrm{c}}}\delta(\boldsymbol{k}-\boldsymbol{k}')\langle u_{n'\boldsymbol{k}}|\nabla_{\boldsymbol{k}}u_{n\boldsymbol{k}}\rangle$ where $|\psi_{n\boldsymbol{k}}\rangle$ is the Bloch state, we arrive at

$$\mathcal{I}^{(2)}_{xy}=-\frac{1}{\pi}\mathrm{Im}\int_{\mathrm{BZ}}\mathrm{d}\boldsymbol{k}\sum_{n\in\mathrm{occ}}\sum_{n'\notin\mathrm{occ}}\left(\tilde{\varepsilon}_{n'\boldsymbol{k}}+\tilde{\varepsilon}_{n\boldsymbol{k}}\right)^2\langle\psi_{n\boldsymbol{k}}|x|\psi_{n'\boldsymbol{k}}\rangle\langle\psi_{n'\boldsymbol{k}}|y|\psi_{n\boldsymbol{k}}\rangle. \quad (9)$$

Using $\tilde{H}|\psi_{n\boldsymbol{k}}\rangle=\tilde{\varepsilon}_{n\boldsymbol{k}}|\psi_{n\boldsymbol{k}}\rangle$, we can write

$$\mathcal{I}^{(2)}_{xy} = -\frac{1}{\pi}\mathrm{Im}\int_{\mathrm{BZ}}\mathrm{d}\boldsymbol{k}\sum_{n\in\mathrm{occ}}\sum_{n'\notin\mathrm{occ}}\Big(\langle\psi_{n\boldsymbol{k}}|x\tilde{H}^2|\psi_{n'\boldsymbol{k}}\rangle\langle\psi_{n'\boldsymbol{k}}|y|\psi_{n\boldsymbol{k}}\rangle +\langle\psi_{n\boldsymbol{k}}|x|\psi_{n'\boldsymbol{k}}\rangle\langle\psi_{n'\boldsymbol{k}}|y\tilde{H}^2|\psi_{n\boldsymbol{k}}\rangle+2\langle\psi_{n\boldsymbol{k}}|x\tilde{H}|\psi_{n'\boldsymbol{k}}\rangle\langle\psi_{n'\boldsymbol{k}}|y\tilde{H}|\psi_{n\boldsymbol{k}}\rangle\Big). \quad (10)$$

With the definition of projector operators $P = \frac{A_c}{(2\pi)^2}\sum_{n\in\text{occ}}\int_{\text{BZ}} \mathrm{d}\boldsymbol{k}\,|\psi_{n\boldsymbol{k}}\rangle\langle\psi_{n\boldsymbol{k}}|$ and $Q = I - P$, where the integral is over the first Brillouin zone, we have obtained the final formula as

$$\mathcal{I}_{xy}^{(2)} = -\frac{4\pi}{A_c}\mathrm{Im}\mathrm{Tr}\big(PxQ\tilde{H}^2QyP + PxQyP\tilde{H}^2 - 2\tilde{H}PyQ\tilde{H}QxP\big). \tag{11}$$

Here we have used

$$\mathrm{Im}\mathrm{Tr}\left(Px\tilde{H}Qy\tilde{H}P\right) = -\mathrm{Im}\mathrm{Tr}\left(P\tilde{H}yQ\tilde{H}xP\right), \tag{12}$$

where $Px\tilde{H}Qy\tilde{H}P$ and $P\tilde{H}yQ\tilde{H}xP$ are Hermitian conjugates of each other. Compared with the real part, the only difference lies in the sign of Eq. (10). Noticing the sign difference in Eqs. (2) and (3), we emphasize that the identity in Eq. (12) combined with $\mathrm{Re}\left(Px\tilde{H}Qy\tilde{H}P\right) = \mathrm{ReTr}\left(P\tilde{H}yQ\tilde{H}xP\right)$ is a key step to provide a unified formula for both the real and imaginary parts.

Equations (5)–(7) form the basis for carrying out calculations of GQGTs in real-space lattices with disorder. The motivations for introducing disorder are two-fold. First, it is to check disorder effects on the behaviors of these physical quantities. Second, it is interesting to find out whether the non-trivial inequality in Eq. (4) is still valid in a disordered lattice.

4. Model and methods

We demonstrate the effects of disorder by using the Haldane model as an example. The Hamiltonian in real space is written as[23]

$$H_0 = t_1\sum_{\langle i,j\rangle} c_i^\dagger c_j + t_2\sum_{\langle\langle i,j\rangle\rangle} \mathrm{e}^{\mathrm{i}\nu_{ij}\phi}c_i^\dagger c_j + \sum_i \tilde{M}\xi_i c_i^\dagger c_i. \tag{13}$$

Here, $c_i^{(\dagger)}$ annihilates (creates) an electron on site i, t_1 is the real nearest-neighbor hopping on pairs $\langle i,j\rangle$, and t_2 is the next-nearest-neighbor hopping on pairs $\langle\langle i,j\rangle\rangle$ with a complex phase $\mathrm{e}^{\mathrm{i}\nu_{ij}\phi}$, in which ϕ is the magnetic flux, and $\nu_{ij} = \pm 1$ distinguishes clockwise from counterclockwise hopping paths inside a unit cell, breaking time-reversal symmetry without a net magnetic field. $\tilde{M}$ is a staggered sublattice potential with $\xi_i = +1$ on sublattice A and -1 on sublattice B. The model exhibits a topological phase transition as a function of M and ϕ. When $t_2 \neq 0$ and $\phi \neq 0, \pi$, the system enters the phase of a Chern insulator with the absolute value of the Chern number $|C| = 1$ provided that $|\tilde{M}| < 3\sqrt{3}t_2|\sin\phi|$. Outside this regime, the system is a trivial band insulator. We introduce onsite disorder to the system as

$$H_{\text{dis}} = \sum_i \Delta_i c_i^\dagger c_i. \tag{14}$$

Here, Δ_i denotes the onsite disorder potential uniformly distributed in the interval $[-\Delta, \Delta]$ with strength $\Delta > 0$. We calculate the physical quantities in Eqs. (5)–(7) by averaging over different disorder configurations.

5. Results and discussion

We present our results for the physical quantities of the Haldane model in Eqs. (5)–(7) for different onsite disorder strengths. We set $t_1 = 1$, which is the energy unit, $t_2 = \frac{1}{3\sqrt{3}}$, $\phi = \frac{\pi}{2}$, and fix the chemical potential just on the top of the valence band. For the Haldane model without disorder, the topological phase transition happens at $\tilde{M} = 1$, which is clearly indicated by the Chern number for $\Delta = 0$ in Fig. 1(a). $\sqrt{\det R^{(0)}}$ for $\Delta = 0$ can also signify the topological phase transition, consistent with results in Refs. [13,24,28]. When onsite disorders are turned on, both the Chern number and $\sqrt{\det R^{(0)}}$ in Figs. 1(a) and 1(b) show that the topologically non-trivial area is enlarged. It can be attributed to the effective change of the staggered potential M due to onsite disorders, as formulated in Ref. [29].

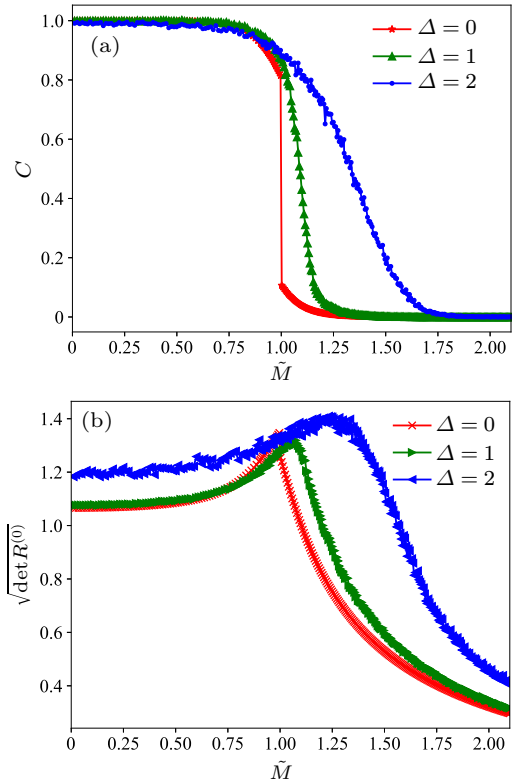

Fig. 1. The Chern number and $\sqrt{\det R^{(0)}}$ for the Haldane model versus $\tilde{M}$ for different disorder strengths. The lattice size is 24×24. $t_1 = 1$, $t_2 = \frac{1}{3\sqrt{3}}$, and $\phi = \frac{\pi}{2}$. For disordered cases, these quantities are calculated by averaging over 256 configurations. We fix the chemical potential just on the top of the valence band.

In Fig. 2, we show the orbital magnetization M_z and $\sqrt{\det R^{(1)}}$ for the Haldane model versus $\tilde{M}$ for different disorder strengths. In the calculations we fix the chemical potential just on the top of the valence band, and it means that the chemical potential may be changed due to parameter variations. For

$\Delta = 0$, we observe that the orbital magnetization decreases linearly with $\tilde{M}$ and vanishes when the gap is closed, consistent with its formula in Eq. (1) in the momentum space, in contrast to the quadratic decrease with $\tilde{M}$ of the energy magnetization $M_{E,z}$ in Fig. 3(a). Meanwhile, $\sqrt{\det R^{(1)}}$ in Fig. 2(b) also shows the phase transition at $\tilde{M} = 1$. When the disorder is turned on, we see the trend that the phase transition point is shifted to $\tilde{M}$ greater than 1. Similar behaviors are also observed for $\sqrt{\det R^{(2)}}$ in Fig. 3(b). However, when the disorder strength is increased to 2, the phase transition is largely smeared out due to strong fluctuations induced by disorder.

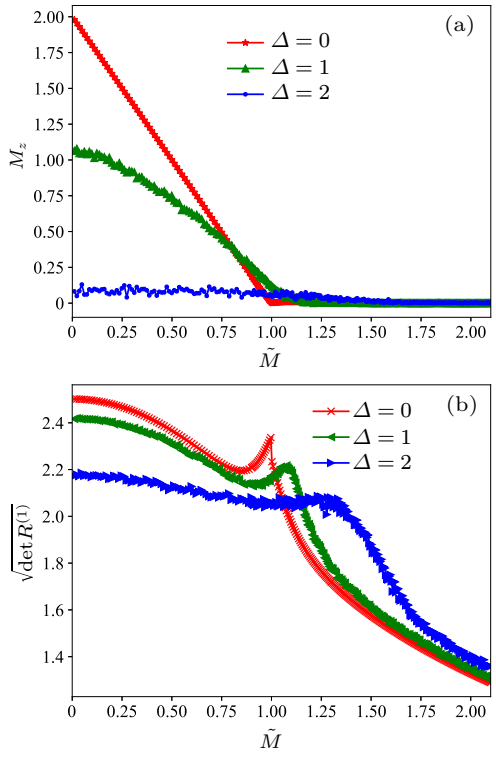

Fig. 2. The orbital magnetization M_z and $\sqrt{\det R^{(1)}}$ for the Haldane model versus $\tilde{M}$ for different disorder strengths. We fix the chemical potential just on the top of the valence band. The other parameters are the same as those in Fig. 1.

Importantly, we point out that the inequality in Eq. (4) is still valid in disordered cases, as shown clearly in Figs. 1 and 2. In disordered cases, the semi-positive definite property is valid for every disorder configuration, and on average the inequality in Eq. (4) still works. Surprisingly, we see that the inequality in Eq. (4) is satisfied for $j = 2$. For the two-band Haldane model, the real and imaginary parts of $\mathcal{Q}^{(2)}_{\alpha\beta}$ can be written as

$$\mathrm{Re}\mathcal{Q}^{(2)}_{\alpha\beta} = \int_{\mathrm{BZ}} \mathrm{d}\boldsymbol{k} \mathrm{Re}\left(\tilde{\varepsilon}_{o\boldsymbol{k}} - \tilde{\varepsilon}_{u\boldsymbol{k}}\right)^2 \mathrm{Re}\mathcal{Q}^{(0)}_{\alpha\beta,\boldsymbol{k}}, \quad (15)$$

$$\mathrm{Im}\mathcal{Q}^{(2)}_{\alpha\beta} = \int_{\mathrm{BZ}} \mathrm{d}\boldsymbol{k} \mathrm{Im}\left(\tilde{\varepsilon}_{o\boldsymbol{k}} + \tilde{\varepsilon}_{u\boldsymbol{k}}\right)^2 \mathrm{Im}\mathcal{Q}^{(0)}_{\alpha\beta,\boldsymbol{k}}, \quad (16)$$

where we have defined $\mathcal{Q}^{(0)}_{\alpha\beta,\boldsymbol{k}} = \frac{1}{\pi}\left\langle \frac{\partial u_{o\boldsymbol{k}}}{\partial k_\beta} \middle| u_{u\boldsymbol{k}} \right\rangle \left\langle u_{u\boldsymbol{k}} \middle| \frac{\partial u_{o\boldsymbol{k}}}{\partial k_\alpha} \right\rangle$, and the subscripts o and u stand for occupied and unoccupied, respectively. Equations (15) and (16) can be treated as a linear combination of $\mathrm{Re}\mathcal{Q}^{(0)}_{\alpha\beta,\boldsymbol{k}}$ and $\mathrm{Im}\mathcal{Q}^{(0)}_{\alpha\beta,\boldsymbol{k}}$ with different coefficients. If all the coefficients are ones, the constraint due to the semi-positive definiteness of $\mathcal{Q}^{(0)}_{\alpha\beta}$ is followed. Here, for the uniformly distributed disorder we have implemented, on average the particle–hole symmetry of the band structure is preserved; for most momenta $\boldsymbol{k}$, the relation $(\tilde{\varepsilon}_{o\boldsymbol{k}} - \tilde{\varepsilon}_{u\boldsymbol{k}})^2 > (\tilde{\varepsilon}_{o\boldsymbol{k}} + \tilde{\varepsilon}_{u\boldsymbol{k}})^2$ is satisfied, which in fact strengthens the positive contribution of $\mathrm{Re}\mathcal{Q}^{(2)}_{\alpha\beta}$. As a result, the constraint imposed by the semi-positive definiteness is followed.

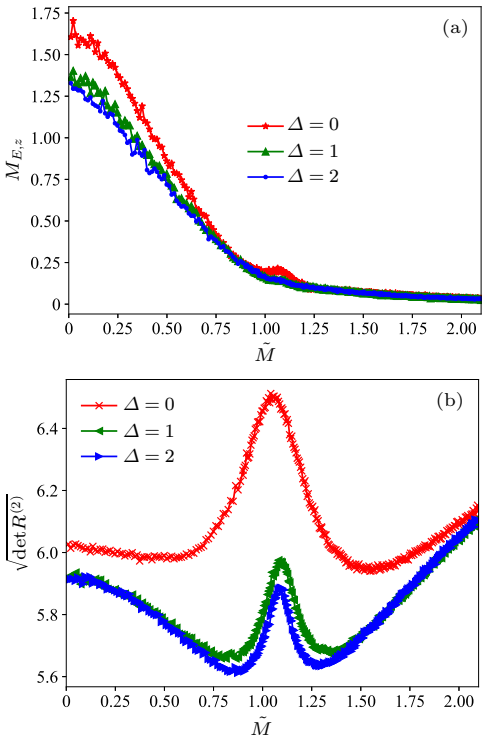

Fig. 3. The energy magnetization $M_{E,z}$ and $\sqrt{\det R^{(2)}}$ for the Haldane model with different disorder strengths. We fix the chemical potential just on the top of the valence band. The other parameters are the same as those in Fig. 1.

In Figs. 4 and 5, we fix the chemical potential at $\mu = 0$. Our observations are as follows. The inequality in Eq. (4) is valid for $j = 1$ even though there are disorders. Furthermore, we find that the orbital magnetization M_z in Fig. 4(a) is almost zero, consistent with expectation from Eq. (1) in the momentum space. Finally, in both Figs. 4(a) and 5(a), we see that the feature at the phase transition is smeared out by disorders, in contrast to $\sqrt{\det R^{(1)}}$ and $\sqrt{\det R^{(2)}}$ in Figs. 4(b) and 5(b), which are not affected by the chemical potential.

We now comment on the experimental measurement of the energy magnetization and energy Drude weight. We can decompose the energy magnetization $M_{E,z}$ into three distinct contributions as follows:

$$M_{E,z} = \int_{\mathrm{BZ}} \mathrm{d}\boldsymbol{k} \sum_{n\in\mathrm{occ}} \left(M^E_{z,n\boldsymbol{k}} + 4M_{z,n\boldsymbol{k}} + 2\Omega_{z,n\boldsymbol{k}}\right), \quad (17)$$

where the energy magnetic moment

$$M^E_{z,n\boldsymbol{k}} = -\frac{1}{\pi}\mathrm{Im}\left\langle \frac{\partial u_{n\boldsymbol{k}}}{\partial k_x} \middle| \left(H - \varepsilon_{n\boldsymbol{k}}\right)^2 \middle| \frac{\partial u_{n\boldsymbol{k}}}{\partial k_y} \right\rangle,$$

the orbital magnetic moment

$$M_{z,n\boldsymbol{k}} = -\frac{1}{\pi}\mathrm{Im}\left(\varepsilon_{n\boldsymbol{k}} - \mu\right)\left\langle \frac{\partial u_{n\boldsymbol{k}}}{\partial k_x}\middle| \left(H - \varepsilon_{n\boldsymbol{k}}\right)\middle|\frac{\partial u_{n\boldsymbol{k}}}{\partial k_y}\right\rangle,$$

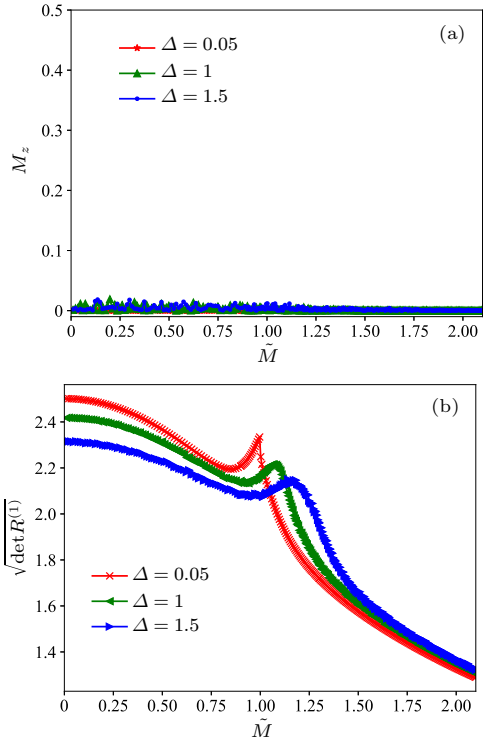

Fig. 4. The orbital magnetization M_z and $\sqrt{\det R^{(1)}}$ for the Haldane model versus $\tilde{M}$ for different disorder strengths. We set the chemical potential at $\mu = 0$, and average over 1024 disordered configurations. The other parameters are the same as those in Fig. 1.

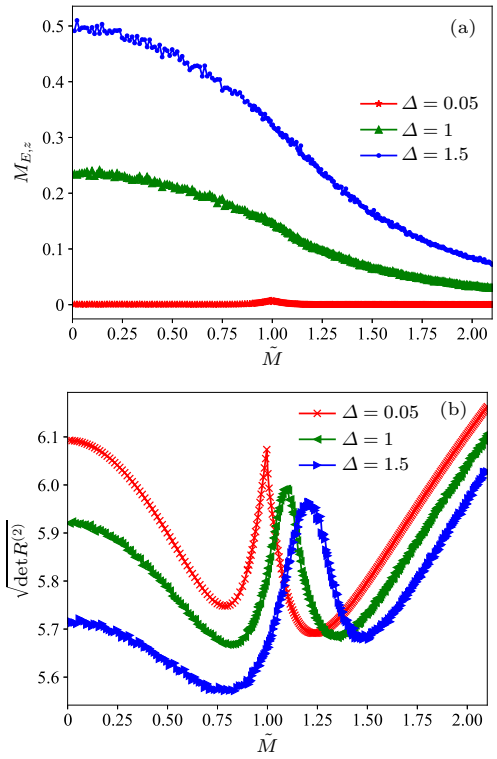

Fig. 5. The energy magnetization $M_{E,z}$ and $\sqrt{\det R^{(2)}}$ for the Haldane model versus $\tilde{M}$ for different disorder strengths. We set the chemical potential at $\mu = 0$, and average over 1024 disordered configurations. The other parameters are the same as those in Fig. 1.

and the Berry curvature $\Omega_{z,n\boldsymbol{k}} = -\frac{2}{\pi}\mathrm{Im}\left\langle \frac{\partial u_{n\boldsymbol{k}}}{\partial k_x}\middle|\frac{\partial u_{n\boldsymbol{k}}}{\partial k_y}\right\rangle$. The orbital magnetic moment can be measured by the x-ray magnetic circular dichroism,[30] while the Berry curvature can be measured via their relationship with the anomalous Hall effect.[31] In Ref. [32], the authors proposed that, via the entanglement brought by the electron–phonon coupling, the energy Drude weight $D^E_{z,n\boldsymbol{k}}$ which is from the real part of $\mathcal{Q}^{(2)}_{\alpha\beta}$, and the energy magnetic moment $M^E_{z,n\boldsymbol{k}}$ can be measured by exploring their relationship with the linear phonon dichroism and circular phonon dichroism, respectively.

6. Summary and outlook

To sum up, we carry out a generalization of the usual QGT to include the energy magnetization. By formulating these quantities in real space, we explore their properties when disorder is introduced. With the disordered Haldane model as an example, we find that (1) the topologically non-trivial area is enlarged due to disorder, and (2) the inequality due to the semi-positive properties of these quantities is still valid in disordered cases, which we attribute to its validity for every configuration. The generalization to other lattice models is straightforward. In the future, we plan to explore more interesting lattice models with different types of disorder.

Acknowledgements

This project is supported by the National Natural Science Foundation of China (Grant Nos. U2032164 and 12174394) and the Start-up Fund from Anhui University in China.

References

[1] Souza I, Wilkens T and Martin R M 2000 *Phys. Rev. B* **62** 1666
[2] Resta R 2011 *Eur. Phys. J. B* **79** 121
[3] Xiao D, Chang M C and Niu Q 2010 *Rev. Mod. Phys.* **82** 1959
[4] Provost J P and Vallee G 1980 *Commun. Math. Phys.* **76** 289
[5] Gao A, Nagaosa N, Ni N and Xu S Y 2025 Preprint 2508.00469
[6] Yu J, Bernevig B A, Queiroz R, Rossi E, Törmä P and Yang B J 2025 *npj Quantum Mater.* **10** 101
[7] Verma N, Moll P J W, Holder T and Queiroz R 2026 *Nat. Rev. Phys.* **8** 226
[8] Törmä P 2023 *Phys. Rev. Lett.* **131** 240001
[9] Wang N, Kaplan D, Zhang Z, Holder T, Cao N, Wang A, Zhou X, Zhou F, Jiang Z, Zhang C, Ru S, Cai H, Watanabe K, Taniguchi T, Yan B and Gao W 2023 *Nature* **621** 487
[10] Gao A, Liu Y F, Qiu J X, Ghosh B, Trevisan T V, Onishi Y, Hu C, Qian T, Tien H J, Chen S W, Huang M, Bérubé D, Li H, Tzschaschel C, Dinh T, Sun Z, Ho S C, Lien S W, Singh B, Watanabe K, Taniguchi T, Bell D C, Lin H, Chang T R, Du C R, Bansil A, Fu L, Ni N, Orth P P, Ma Q and Xu S Y 2023 *Science* **381** 181
[11] Yu J, Ciccarino C J, Bianco R, Errea I, Narang P and Bernevig B A 2024 *Nat. Phys.* **20** 1262
[12] Peotta S and Törmä P 2015 *Nat. Commun.* **6** 8944
[13] Ozawa T and Mera B 2021 *Phys. Rev. B* **104** 045103
[14] Mera B and Ozawa T 2021 *Phys. Rev. B* **104** 045104
[15] Roy R 2014 *Phys. Rev. B* **90** 165139
[16] Onishi Y and Fu L 2024 *Phys. Rev. X* **14** 011052
[17] Liu Z, Zhang Z F, Zhu Z G and Su G 2024 *Phys. Rev. B* **110** 245419

[18] Romeral J M, Cummings A W and Roche S 2025 *Phys. Rev. B* **111** 134201
[19] Shi J, Vignale G, Xiao D and Niu Q 2007 *Phys. Rev. Lett.* **99** 197202
[20] Qin T, Niu Q and Shi J 2011 *Phys. Rev. Lett.* **107** 236601
[21] Resta R 2018 *J. Phys.: Condens. Matter* **30** 414001
[22] Bermond B, Gavensky L P, Defossez A and Goldman N 2026 Preprint 2511.21599
[23] Haldane F D M 1988 *Phys. Rev. Lett.* **61** 2015
[24] Shinada K and Nagaosa N 2025 *Phys. Rev. B* **112** 155158
[25] Bianco R and Resta R 2013 *Phys. Rev. Lett.* **110** 087202
[26] Bianco R and Resta R 2016 *Phys. Rev. B* **93** 174417
[27] Bianco R and Resta R 2011 *Phys. Rev. B* **84** 241106(R)
[28] Thonhauser T and Vanderbilt D 2006 *Phys. Rev. B* **74** 235111
[29] Groth C W, Wimmer M, Akhmerov A R, Tworzydło J and Beenakker C W J 2009 *Phys. Rev. Lett.* **103** 196805
[30] Chen C T, Idzerda Y U, Lin H J, Smith N V, Meigs G, Chaban E, Ho G H, Pellegrin E and Sette F 1995 *Phys. Rev. Lett.* **75** 152
[31] Yao Y, Kleinman L, MacDonald A H, Sinova J, Jungwirth T, Wang D S, Wang E and Niu Q 2004 *Phys. Rev. Lett.* **92** 037204
[32] Li D, Yang G, Qin T, Zhou J and Yao Y 2025 Preprint 2511.16141